Fuel Processing Technology 96 (2012) 104–115

Contents lists available at SciVerse ScienceDirect

Fuel Processing Technology

journal homepage: www.elsevier.com/locate/fuproc

Chemical looping combustion of a Chinese anthracite with Fe_2O_3-based and CuO-based oxygen carriers

Baowen Wang [a,b,*], Haibo Zhao [a], Ying Zheng [a], Zhaohui Liu [a], Rong Yan [c], Chuguang Zheng [a]

[a] State Key Laboratory of Coal Combustion, Huazhong University of Science and Technology, Wuhan, 430074, PR China
[b] College of Electric Power, North China University of Water Conservancy and Hydroelectric Power, Zhengzhou, 450011, PR China
[c] Institute of Environmental Science and Engineering, Nanyang Technological University, Innovation Center, Block 2, Unit 237, 18 Nanyang Drive, 637723, Singapore

ARTICLE INFO

Article history:
Received 27 August 2011
Received in revised form 1 December 2011
Accepted 25 December 2011
Available online 17 January 2012

Keywords:
Chemical looping combustion (CLC)
Anthracite coal
CuO/Al_2O_3 and Fe_2O_3/Al_2O_3 oxygen carrier
TGA

ABSTRACT

Chemical looping combustion (CLC) of coal has received great attention for its verified advantage in the inherent separation of CO_2 without great cost penalty. It would be meaningful to adopt anthracite as fuel for CLC application in China due to its abundant reserve in China and also a great challenge for its low reactivity. A typical Chinese anthracite as Yang Quan (YQ) coal was selected in this research as a model fuel and its reaction with both synthesized CuO/Al_2O_3 and Fe_2O_3/Al_2O_3 oxygen carriers (OCs) was performed in a thermogravimetric analyzer (TGA) to investigate the reaction peculiarities involved. Fourier transform infrared spectroscopy (FTIR) was used to in-situ detect the emitted gasses from TGA. Field scanning electron microscopy/energy-dispersive X-ray spectrometry (FSEM-EDX) was used to study the morphology and elemental compositions present in the solid residues collected from the reaction of YQ with these two OCs, and the related phase was identified by X-ray diffraction (XRD). In order to further explore the reaction mechanisms involved, a more realistic reaction system with 426 species was designed for thermodynamic simulation. Through all these measures, two reaction stages were observed for the reaction of YQ with Fe_2O_3/Al_2O_3 or CuO/Al_2O_3 at 300–600 °C and 600–850 °C after dehydration, respectively. The maximum weight loss rate for YQ with CuO/Al_2O_3 at the second stage was pronounced enough to reach up to 2.8 wt.%/min, greatly higher than that of YQ with Fe_2O_3/Al_2O_3. The mixture conversion index for YQ with CuO/Al_2O_3 was far bigger than that of YQ with Fe_2O_3/Al_2O_3, which further indicated that CuO/Al_2O_3 was more suitable to YQ in CLC. At these two stages throughout 400 to 1100 °C, CuO and $CuAl_2O_4$ contained in CuO/Al_2O_3 OC were mainly reduced to Cu and Cu_2O or $CuAlO_2$ and Al_2O_3 by transfer of the lattice oxygen [O] involved to YQ in a sequential mode; however, above 800 °C, Cu_2O and $CuAlO_2$ were also produced through direct decomposition of CuO or $CuAl_2O_4$ by emission of gaseous oxygen O_2, which was beneficial to the direct combustion of coal. During reaction of YQ with CuO/Al_2O_3 OC, active CuO was found to tend to react with various sulfur species produced from YQ pyrolysis and formed to Cu_2S, but the Al_2SiO_5 was formed through the interaction of Al_2O_3 with SiO_2 in the YQ, which resulted in the loss of the inert support involved in the CuO/Al_2O_3 OC and further degraded its reactivity to YQ due to the lower resistance to sintering.

1. Introduction

It is of urgent necessity to decrease CO_2 emission from fossil fuel combustion, especially coal, to protect the environment from the greenhouse effect. There currently exist three methods and techniques to capture CO_2 from coal combustion, such as pre-combustion, oxy-fuel combustion and post-combustion. In comparison to all these techniques available with a great energy consumption and cost penalty, chemical looping combustion (CLC) has instigated great interest for its verified advantages, such as the inherent separation of CO_2 without any extra energy consumption and thorough eradication of the formation of thermal NO_x [1]. In CLC, coal is firstly introduced into a fuel reactor (FR) and fully oxidized with oxygen carrier (OC) instead of air. At its full conversion, pure CO_2 would be available to easy sequestration after condensation of the exit gas from FR, and any extra gas separation process is avoided. Finally, the reduced OC is transported back to an air reactor (AR) and oxidized by air for another cycle of reaction with coal in FR [2–4].

Most research to date on CLC is mainly concentrated on gaseous fuel, and CLC application with solid fuels, especially coal, is still limited [5]. Several investigations from different institutions had confirmed the feasibility of direct use of coal as the fuel for CLC application [2,4,6]. It was found that full conversion of coal is one of the key issues in CLC of coal to obtain CO_2-enriched gas stream for the later sequestration and the main rate-limited step involved was

* Corresponding author at: State Key Laboratory of Coal Combustion, Huazhong University of Science and Technology, Wuhan, 430074, PR China. Tel.: +86 27 87542417; fax: +86 27 87542616.
E-mail address: david-wn@163.com (B. Wang).

0378-3820/$ – see front matter © 2011 Elsevier B.V. All rights reserved.
doi:10.1016/j.fuproc.2011.12.030

actually the gasification of coal, especially that of the left coal char, instead of the reduction of OC with the coal gasification products in situ generated. Lieon, et al. [3,7] systematically studied the reaction between coal of different volatile contents and Fe_2O_3-based OC, and found out that the reaction rate was generally determined by the volatile content in coal and more reactive coal had a higher reaction rate. Dennis et al. [8,9] performed the reaction of CuO-based OC with coal of different rank and indicated that low-rank lignite should be much better to ensure its full conversion than a bituminous coal for CLC application. And all these researchers from different institutions concluded that more reactive coal with low rank should be preferred to CLC of coal [3,7–9], but anthracite in China is abundant with great recoverable reserve amounting to 1200 billion ton and annual yield ranked the first in the World [10,11], though such a coal is a high rank coal with the low content of volatile matters and considered as less reactive [12]. Therefore, it would be meaningful and a great challenge to adopt anthracite as fuel for CLC application in China and investigate the reaction peculiarity of anthracite with different OCs.

OC was the basis for CLC and acted as oxygen conductor as well as energy carrier in CLC, which is composed of the active metal oxides and inert support [13]. Till now, Fe_2O_3, CuO and NiO are widely used in CLC as the active oxides, and a variety of inert materials have been reported as the inert supports for OC, such as Al_2O_3, SiO_2, ZrO_2, etc. Among which, Al_2O_3 is recognized as one of the most promising supports [14]. But for the active oxides in OC, NiO was found to have high reactivity to coal [4,6,15,16], but the potential carcinogenic tendency limited its future application in CLC. Fe_2O_3 OC was found active enough to react with coal, but lower than NiO in the real coal-based CLC system [2,3,7,17]. In view of maintaining a sufficient FR temperature for a high gasification rate, CuO has been highly appraised and intensively studied for the exothermic characteristics of its reduction reaction with various fuels [18–22]. But in comparison to the extensive research on these active oxides, little effort was made to study the effect of inert support during the reaction of coal with OC. Experiment on the dilution of carbon and CuO mixture by inert quartz indicated that quartz was disadvantageous to the reaction of carbon with CuO [23]. Therefore, research on the inert support involved in OC on its reaction with coal is limited and worthwhile to be further explored.

After the full reaction of coal with metal OC, effective separation of the reduced OC from coal ash is also a great concern [2]. Interaction between the reduced OC and ash components would bring about some inert compounds formed and deteriorated its reactivity [2,16,21,24]. As a detrimental consequence, the melting point of the formed ash was lowered and agglomeration of the reduced OC with ash possibly occurred, which incurred the great difficulty to separate the reduced OC from the formed coal ash. Therefore, it is also important to understand the ash effect on the reactivity of OC and the possible interaction mechanisms involved.

In this study, both Fe_2O_3/Al_2O_3 and CuO/Al_2O_3 OCs were synthesized using the novel sol–gel combustion synthesis (SGCS) and their reaction stabilities were evaluated by four cycles of the reduction with H_2 and then oxidation with air. Reaction of the synthesized OCs with a Chinese high ranked coal as Yang Quan (YQ) anthracite was investigated using TGA to explore their reaction peculiarities. The emitted gasses were analyzed using FTIR coupled with TGA. Morphology and chemical components of the reduced solid products were characterized using FSEM-EDX, and their phases were further identified by XRD. Finally, thermodynamic simulation of the reduction of the selected Chinese anthracite with CuO/Al_2O_3 was conducted to explore the reaction mechanism involved. The overall aim of this research was to provide useful information to adopt the abundant anthracite coal in China as the fuel in a practical CLC system.

2. Experimental procedures

2.1. Materials and characterization

The OCs used in this research, including both Fe_2O_3/Al_2O_3 and CuO/Al_2O_3 with the mass ratio of the active oxide Fe_2O_3 or CuO to the inert support Al_2O_3 set as 4:1, were synthesized by the novel sol–gel combustion synthesis (SGCS) method, which displayed great advantages for its rapidity and simplicity of the synthesizing process, lower energy requirement and good resistance to sintering by combining both the sol–gel synthesis and combustion synthesis methods, and was promising to produce OC with good performance for CLC application [14]. The hydrated nitrates and urea were used as the precursors. And the detailed preparation procedure for these OCs was elaborated in our previous research [14].

After the desired OC was prepared, the synthesized OC samples were further ground and sieved to collect the samples in 63–106 μm size for the ensuing use. Phase identification of the as-synthesized Fe_2O_3/Al_2O_3 and CuO/Al_2O_3 OCs was performed through X-ray diffractor (XRD) (X'Pert PRO, The Netherlands) with 40 kV and 40 mA Cu Kα radiation at a scanning rate of 1°/min. And their averaged crystalline sizes of the synthesized OCs were further evaluated employing the Scherrer formula below.

$$D = 0.9\lambda/(\beta\cos\theta) \quad (1)$$

where D is the crystallite size in nm, λ is the radiation wavelength (0.15406 nm for Cu *K*α), θ is the diffraction angle and β is the corrected halfwidth for instrument broadening. Meanwhile, specific surface area and pore size distribution of the synthesized OCs were derived on the adsorption analyzer (Micrometrics ASAP 2020,USA) at −196 °C.

For the fuel adopted in this research, a typical Chinese coal of high rank as Yang Quan anthracite was adopted and designed as YQ below. After drying, grinding and sieving, the YQ sample in the size range of 63–106 μm was collected and used. The sieved coal sample was further characterized using proximate and ultimate analyses as well as ash composition analysis with X-ray fluorescence (XRF, Philips, PW 2400, The Netherlands), as provided in Table 1.

Finally, both the synthesized OCs and as-prepared YQ coal sample were evenly mixed in a laboratory mortar at the designed mass ratio, as described below in Section 2.2.

Table 1
Properties of YQ anthracite studied.

Proximate analysis[a] (wt.%)				Ultimate analysis (wt.%, d[b])					LHV[d] (MJ/kg)
M_{ad}	V_{ad}	A_{ad}	FC_{ad}	C	H	N	S	O[c]	
2.39	8.05	29.24	60.32	64.02	1.81	1.1	0.67	32.40	22.71
Ash analysis of YQ (wt.%)									
SiO_2	Al_2O_3	Fe_2O_3	SO_3	CaO	TiO_2	Co_3O_4	K_2O	MgO	Na_2O
68.49	14.58	4.48	4.10	3.65	0.69	0.52	1.04	0.63	1.24

[a] M: moisture content; V: volatile matters; A: ash content; FC: fixed carbon; ad: air-dried basis; [b]: dry basis; [c]: the O content was determined by difference; [d]: lower heating value.

2.2. Determination of the oxygen excess number Φ for YQ coal sample

Sufficient supply of the OC is very important to ensure the full conversion of coal in the CLC system. To determine the amount of OC to be introduced into the CLC system, the method of coal mass balance was adopted. Similar to the reference [25], from the properties of YQ anthracite in Table 1, the weight fractions of both hydrogen and oxygen in the moisture were deducted. If 1 kg of YQ coal sample was used, the content of different atoms (including C, H, O, N, S) contained in YQ could be determined and the relative chemical formula was represented as $C_\alpha H_\beta S_\gamma O_\delta (N_2)_\nu$. If CuO/Al_2O_3 OC was selected as a model OC, and its fully reduced counterpart was supposed as Cu and Al_2O_3 when coal being fully converted, the reduced reaction of CuO/Al_2O_3 OC with YQ coal could be depicted below.

$$C_\alpha H_\beta S_\gamma O_\delta (N_2)_\nu + (2\alpha+\beta/2+2\gamma-\delta)CuO/Al_2O_3 \rightarrow (2\alpha+\beta/2+2\gamma-\delta)\,(Cu+Al_2O_3) + \alpha CO_2(g) + \beta/2 H_2O(g) + \gamma SO_2(g) + \nu N_2(g) \quad (2)$$

From Eq. (2), the theoretical stoichiometric oxygen needed for the full conversion of YQ is $(2\alpha+\beta/2+2\gamma-\delta)$. Supposing the realistic oxygen contained in OC was Y(O), the oxygen excess number Φ was determined below.

$$\Phi = Y(O)/((2\alpha+\beta/2+2\gamma-\delta)) \quad (3)$$

In Eq. (3), Φ = 1 referred that the OC supplied theoretically just met the oxygen requirement to the full conversion of coal. According to the aforementioned method, the relative chemical formula of YQ of 1 kg could be depicted as $C_{36.8}H_{10.2}N_{0.54}S_{0.144}O_{13.1}$. Then, based on Eqs. (2) and (3), for the reduction of CuO/Al_2O_3 or reference oxide CuO with YQ at Φ = 1, the mass ratios of CuO/Al_2O_3 or CuO to YQ were corresponding to 6.68 and 5.34, respectively. But for the reduction of Fe_2O_3/Al_2O or reference oxide Fe_2O_3 with YQ at Φ = 1, if the active Fe_2O_3 was reduced to Fe_3O_4, the relative mass ratio was determined as 40.21 and 32.17 by Eq. (2), respectively.

2.3. Experimental methods

For OC in CLC, good redox properties and sintering-resistance are of great significance. In order to evaluate the reaction stability of the synthesized Fe_2O_3/Al_2O_3 and CuO/Al_2O_3 OCs over multiple cycles, H_2 was selected as fuel, and four cycles of the reduction of the as-synthesized OCs with 50 vol.% H_2 in balance N_2 and then oxidation with air were performed at 850 °C in the thermogravimetric analyzer (TA 2050, TA Instruments, US). The total gas flow rate was fixed as 50 ml/min. The detailed experimental procedures were described below. Firstly, 15 mg of CuO/Al_2O_3 or Fe_2O_3/Al_2O_3 OC samples were heated in N_2 at 10 °C/min until the final temperature of 850 °C was reached. Then, N_2 flow was switched to H_2 flow, and reduction of the selected OC with H_2 was initiated and sustained for 8 min. Hereafter, N_2 flow was introduced back again to sweep the remaining H_2 away for 2 min to avoid mixing with air to be used later. Finally, air was introduced to start the oxidation of the reduced OC for 3 min. The same processes were repeated for four times. In addition, similar to the four cycles of CuO/Al_2O_3 or Fe_2O_3/Al_2O_3 OC with H_2 and air, four times of such experimental processes for single oxides CuO and Fe_2O_3 were also performed for references.

The reaction characteristics of the synthesized CuO/Al_2O_3 or Fe_2O_3/Al_2O_3 OC with YQ anthracite at the oxygen excess number Φ = 1 were further investigated using the same TGA instrument. The mixture of YQ with CuO/Al_2O_3 or Fe_2O_3/Al_2O_3 was heated from ambient to 150 °C at 10 °C/min and held at this temperature for up to 10 min so as to fully remove the moisture in YQ. Then, it was further heated up to 850 °C at 35 °C/min with duration at this temperature for 10 min to realize the sufficient conversion of coal. N_2 atmosphere was used, and several pre-screening experiments were performed so as to eliminate the potential impact of mass transfer between the gas and solid phases and ensure the reproducible experimental results. The flow rate of N_2 and the total mass for the mixture of YQ coal and OC were determined at 50 ml/min and ~15 mg, respectively.

The evolved gasses from the reaction of YQ with CuO/Al_2O_3 or Fe_2O_3/Al_2O_3 OC in the TGA were firstly dried through a portable tubular gas desiccator full of $Ca(SO_4).2H_2O$, and then in-situ detected by FTIR spectrometer equipped with a deuterated triglycine sulfate (DTGS) detector (BioRad Excalibur Series, model FTS 3000). The scanning range of IR was 4000–500 cm^{-1}, and the resolution and sensitivity were pre-set at 4 cm^{-1} and 1, respectively.

The morphology and elemental composition of the solid products from the reaction of YQ with CuO/Al_2O_3 or Fe_2O_3/Al_2O_3 OC were studied using FSEM (Siron 200, The Netherlands) coupled with an EDX (GENESIS, US) at a magnification of 800 and an accumulated voltage of 30 kV. The formed phases were identified by XRD (X'Pert PRO, The Netherlands) with 40 kV 40 mA Cu Kα (λ = 0.154 Å) radiation and the step-scanned range of 10–90°.

2.4. Conversion of CuO or Fe_2O_3-based OC with YQ coal

In order to illuminate the transfer of lattice oxygen involved in the CuO/Al_2O_3 or Fe_2O_3/Al_2O_3 OC and the transformation of YQ during its reaction with the OC used, two conversion indexes were defined and described below.

One conversion index for the mixture between YQ coal and the OC used, was defined as X_{YQ-OC}, to reflect the interaction of YQ coal with OC [26–29],

$$X_{YQ-OC}(t) = \frac{W_{YQ-OC}(t=0) - W_{YQ-OC}(t)}{x_1 \Delta W_{OC} + x_2 \Delta W_{YQ}} \quad (4)$$

$$f = x_1/x_2 \quad (5)$$

where X_{YQ-OC} is the mixture conversion index for YQ with CuO/Al_2O_3 or Fe_2O_3/Al_2O_3 OC used in this research(%); W_{YQ-OC} (t = 0) and W_{YQ-OC} (t) are the initial and instantaneous weight loss for the mixture (wt.%); x_1 and x_2 represent the mass fractions of OC and YQ coal in their mixture (wt.%), respectively, arising from the mass ratio of different OCs to YQ determined in the previous

Table 2
Structural characteristics of the synthesized CuO/Al_2O_3 and Fe_2O_3/Al_2O_3 OCs by SGCS.

Sample	BET surface area[a] (m^2/g)	Porosity[a] (cm^3/g)	Average pore size[a] (nm)	Main species[b]	Crystalline size[c] (nm)
CuO	0.5920	0.000468	15.9448	CuO	107.3
CuO/Al_2O_3	1.1415	0.005245	8.9589	CuO	79.9
				$CuAl_2O_4$	108.4
Fe_2O_3/Al_2O_3	1.8550	0.002150	8.1367	Fe_2O_3	78.7
				α-Al_2O_3	37.8
Al_2O_3	4.8871	0.007394	7.2665	α-Al_2O_3	79.1
Fe_2O_3	0.6823	0.001390	9.3567	Fe_2O_3	89.2

[a]:Measured by the BET method; [b]: Identified by XRD analysis; [c]: Estimated from the Scherrer equation in Eq. (1).

Table 3
Species considered in the HSC calculation for the reaction of CuO/Al_2O_3 with YQ.

Main elements in YQ	C	H	O	N	S
Potential minerals present in YQ	Oxides	Fe_2O_3, Fe_3O_4, FeO; Cu_2O, CuO; $CuFeO_2$; SiO_2; Al_2O_3; CaO, CaO_2; MgO,MgO_2;K_2O, Co_3O_4,CoO; NaO,Na_2O_2;TiO_2,Ti_2O_3,Ti_3O_5,Ti_4O_7, etc.			
	OH-containing compounds	$Fe(OH)_2$, $Fe(OH)_3$; $Cu(OH)_2$; $Al(OH)_3$; $Ca(OH)_2$; $Co(OH)_2$; KOH; $Mg(OH)_2$; NaOH, etc.			
	C-containing compounds	Fe_3C, $Fe_3C(A)$, $FeCO_3$; $CuCO_3$; CaC, $CaCO_3$, CaC_2O_4; K_2CO_3; $MgCO_3$, $MgCO_3\cdot3H_2O$; Na_2CO_3, $NaHCO_3$, $Na_2C_2O_4$, $Na_2CO_3\cdot3NaHCO_3$, $Na_2CO_3\cdot NaHCO_3\cdot2H_2O$; $FeCO_3$, etc.			
	S-containing compounds	CuS, Cu_2S, $CuSO_4$, Cu_2SO_4; $Fe_2(SO_4)_3$, $FeSO_4$, FeS, FeS_2, $CuFeS_2$,CaS,$CaSO_3$,$CaSO_4$; CuS, Cu_2S,$CuSO_4$,Cu_2SO_4; K_2SO_4, etc.			
	Si-containing compounds	FeSi, $FeSi_2$, Fe_3Si, Fe_5Si_3, $FeSiO_3$, Fe_2SiO_4, CaSi,$CaSi_2$,Ca_2Si, $CaSiO_3$, Ca_3SiO_5,Ca_3SiO_7,$CaSiO_4$, etc.			
	Al-containing compounds	$CuAl_2O_4$,$CuAlO_2$;$FeAl_2O_4$; $MgAl_2O_4$; $CaAl_2$, $CaAl_4$, $Ca_2Al_2O_5$, $CaO\cdot2Al_2O_3$, $2CaO\cdot2Al_2O_3$, etc.			
	Ti-containing compounds	FeTi, Fe_2Ti, Fe_2TiO_4, Fe_2TiO_5; $Ca_3Ti_2O_7$, $CaO\cdot TiO_2$, $CaO\cdot3TiO_2$, etc.			
	Intermediates between Si and Al	$Al_2SiO_5(OH)_4$,Al_2SiO_5,$Al_6Si_2O_{13}$, etc. $CaAl_2SiO_6$,$CaAl_2SiO_8$, $Ca_2Al_2SiO_7$,$Ca_2Al_2Si_8O_{21}$, etc. $NaAlSi_3O_8$, $KAlSi_3O_8$, $Mg_2Al_4SiO_{10}$, $Fe_2Al_4Si_5O_{18}$, etc.			
Oxygen carrier		CuO/Al_2O_3			
Gaseous species		CH_4, C_2H_4, C_2H_6, CO, CO_2, COS, CN, CN_2, CS_2; H_2, H_2O, HCN, H_2S; O, O_2; NO,NO_2,N_2O_4,N_2O_5; $S_1\sim S_8$,SO,SO_2,SO_3, etc.			

Section 2.2, and then f is the mass ratio of the OC used to YQ; ΔW_{OC} and ΔW_{YQ} are the maximum weight losses of OC and YQ, respectively.

Another conversion index for the OC alone presented in the mixture of OC with YQ coal was defined as X_{OC}, to reveal the real limiting step involved for the reaction of YQ with OC. Based on the conservation of the total weight throughout the reaction of OC with YQ coal, the OC conversion index could be calculated below.

$$W_{YQ-OC}(t) = x_1 W_{OC}(t) + x_2 W_{YQ}(t) \quad (6)$$

$$X_{OC} = \frac{W_{YQ-OC}(t) - x_2 W_{YQ}(t)}{x_1 \Delta W_{OC}} \quad (7)$$

where $W_{OC}(t)$, $W_{YQ}(t)$ and $W_{YQ-OC}(t)$ are the instantaneous weight losses for the YQ coal, OC and their mixture at the time t. And the meanings of the other characters in Eqs. (6) and (7) were the same as those in Eqs. (4) and (5).

2.5. Thermodynamic simulation of the reaction of CuO/Al_2O_3 OC with YQ

Although thermodynamic equilibrium analysis has great limitations and does not consider kinetic constraints in the real process, such as turbulent mixing and temperature gradients [30], the equilibrium calculation would benefit in a better understanding of the lattice oxygen transfer involved in the OC studied and coal transformation. Based on the minimization of the total Gibbs free energy, the reaction of OC with YQ was simulated using the HSC-Chemistry software 4.1.

According to the properties of YQ in Table 1, including its proximate and ultimate analyses as well as ash analysis, a renewed complex reaction system with 426 species in total was established, as shown in Table 3. Noteworthy is that, similar to our previous study [28], in this equilibrium simulation, the coal was considered to consist of the main matrix elements (such as C, H, N, S and O) as well as various minerals present in coal, and seven categories of potential compounds such as various oxides, OH-, C- or CO_3^{2-}-, S- or SO_4^{2-}-, Si-, Al- and Ti-compounds were subdivided; but furthermore, in this research, various potential intermediates from the interaction of these minerals were also considered, which would make this equilibrium simulation more realistic than others' [15,21], where Siriwardane et al. [21] simulated the interaction between the model fly ash(only SiO_2 and Al_2O_3 involved) with different OCs, while Saha and Bhattacharya [15] simulated the reaction of a Victorian brown coal with NiO without considering the effect of the minerals present in that coal.

3. Results and discussion

3.1. Characterization of the synthesized OCs

3.1.1. Phase and structural analysis of the synthesized OCs

In order to reveal the effect of inert support Al_2O_3 involved in the synthesized OCs, phase compositions identified in the XRD are presented in Fig. 1, and the structural analysis data (including surface area, porosity and average pore size) are listed in Table 2.

From the acquired XRD patterns in Fig. 1, phases involved in the synthesized OCs were identified. It could be found out that the

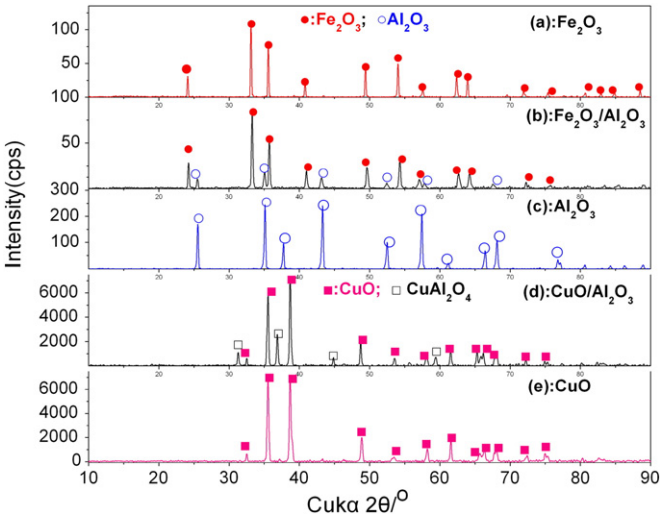

Fig. 1. XRD analysis of the synthesized Fe_2O_3 and CuO-based OCs using SGCS.

synthesized Fe_2O_3/Al_2O_3 was composed of separate phases Fe_2O_3 and α-Al_2O_3, but the actual phases involved in CuO/Al_2O_3 were CuO and spinel phase $CuAl_2O_4$ from the interaction between CuO and Al_2O_3. Meanwhile, based on the XRD patterns obtained in Fig. 1, the averaged crystalline sizes of the active CuO and Fe_2O_3 present in the CuO/Al_2O_3 and Fe_2O_3/Al_2O_3 were calculated using Eq. (1) and provided in Table 2 as 78.7 and 79.9 nm, respectively, smaller than those of separate reference oxides CuO and Fe_2O_3 as 107.3 and 89.2 nm, respectively, which indicated that inert Al_2O_3 introduced effectively improved the sintering-resistance for the CuO and Fe_2O_3 included in the synthesized CuO/Al_2O_3 and Fe_2O_3/Al_2O_3 OCs.

In Table 2, for the structural characteristics of the synthesized OCs using SGCS, both BET surface area and porosity of the reference oxides CuO and Fe_2O_3 were found out as below 0.7 m^2/g and 0.0015 cm^3/g with their pore sizes bigger than 9 nm, but BET surface area and porosity of the inert Al_2O_3 reached as high as 4.8871 m^2/g and 0.007394 cm^3/g with the least average pore size formed as 7.2665 nm, indicating the good resistance of the formed α-Al_2O_3 to sintering. When inert support Al_2O_3 was introduced to the active oxides CuO and Fe_2O_3 at their mass ratio of 1:4, structural characteristics (including surface area, porosity and average pore size) of the synthesized CuO/Al_2O_3 and Fe_2O_3/Al_2O_3 fell within those reference oxides CuO or Fe_2O_3 and support Al_2O_3, which further displayed that the inert support Al_2O_3 really improved the resistance to sintering for the synthesized CuO/Al_2O_3 and Fe_2O_3/Al_2O_3 OCs.

3.1.2. Multiple reduction/oxidation reaction of the synthesized OCs

In order to evaluate the redox characteristics and its resistance to sintering, four cycles of reduction of the synthesized OCs with H_2 and then oxidation with air at 850 °C were performed in the TGA. The experimental results of the mass loss (TG) and the corresponding differential mass loss rate (i.e. DTG) over the four cycles are provided in Fig. 2. Meanwhile, four cycles of the redox process for reference oxides CuO or Fe_2O_3 were performed as well and included in Fig. 2 for comparison.

From Fig. 2, as compared to the reference oxides Fe_2O_3 and CuO, the stability for the reduction of the synthesized Fe_2O_3/Al_2O_3 or CuO/Al_2O_3 OCs over the four cycles at 850 °C was remarkably intensified with 20 wt.% of Al_2O_3 introduced. And the reduction DTG values for Fe_2O_3/Al_2O_3 with H_2 over the four cycles in Fig. 2(a) was stabilized around 26 wt.%/min, less than that of CuO/Al_2O_3 as 33 wt.%/min shown in Fig. 2(b), which proved the better reducibility of CuO/Al_2O_3 than that of Fe_2O_3/Al_2O_3. But the oxidation DTG values for the reduced CuO/Al_2O_3 with air over the four cycles in Fig. 2(b) were stabilized as 43.3 wt.%/min, nearly half of those values for the reduced Fe_2O_3/Al_2O_3 with air (~80 wt.%/min in Fig. 2(a)), which meant that the reduced Fe_2O_3/Al_2O_3 was more easily oxidized back with air than CuO/Al_2O_3. As discussed above, whether for Fe_2O_3/Al_2O_3 or CuO/Al_2O_3, their DTG values for the reduction with H_2 were much smaller than those for oxidation with air. Therefore, more attention should be paid to the reduction of the synthesized OCs by fuel.

3.2. Investigation of the reduction of the synthesized OCs with YQ

3.2.1. TGA-FTIR analysis of the reduction reaction of the synthesized OCs with YQ

The reactions of YQ with the synthesized Fe_2O_3/Al_2O_3 and CuO/Al_2O_3 OC at the oxygen excess number $\Phi = 1$ under N_2 atmosphere were performed in TGA at the heating rate of 35 °C/min. The results of TG and DTG analysis are shown in Fig. 3(a), (c) and (d), respectively. Meanwhile, TG and DTG results for both the baseline test of YQ pyrolysis under N_2 atmosphere and the reactions of YQ with reference oxides Fe_2O_3 and CuO are included in Fig. 3(a)–(d) for comparison.

As the baseline, the YQ pyrolysis under N_2 atmosphere was studied. From the TG curve in Fig. 3(a), below 150 °C, the dehydration occurred with 3.21 wt.% of moisture removed from YQ pyrolysis. And

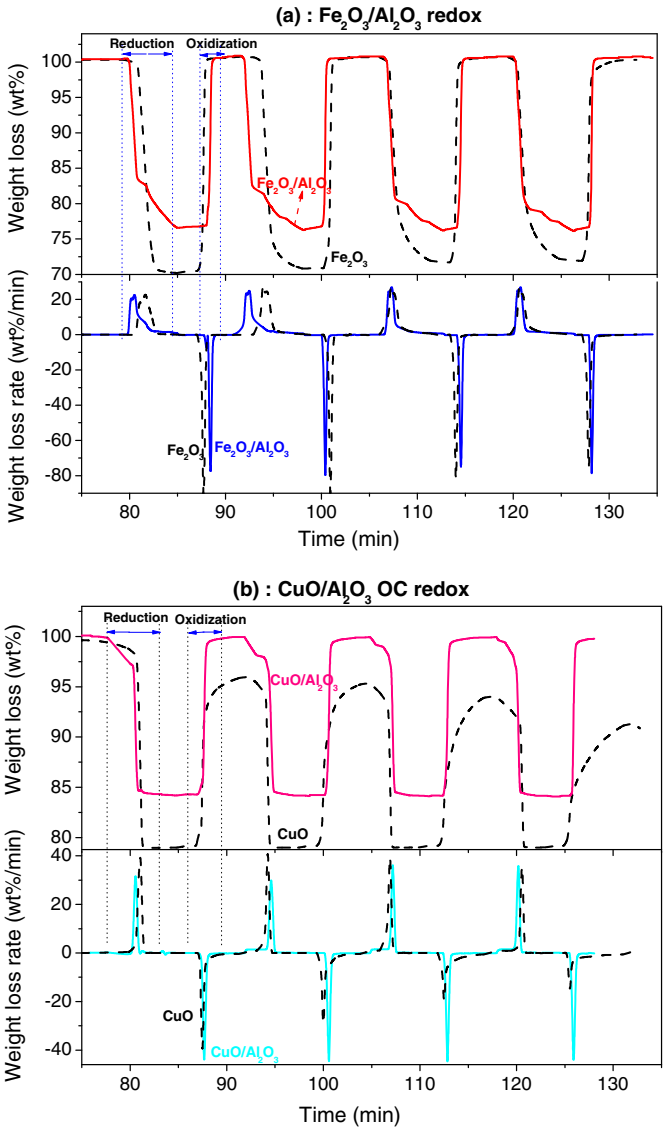

Fig. 2. Four times of redox reactions with H_2 (50 vol.%) and air: (a) Fe_2O_3/Al_2O_3 OC; and (b) CuO/Al_2O_3 OC.

then, over 150 °C, based on the DTG curve in Fig. 3(b), YQ pyrolysis were observed to experience two distinct stages with the corresponding characteristic temperatures T_m (i.e. the peak temperature in relative to the DTG maximum) centering around 531.5 and 695.9 °C, respectively. At the first stage around 150–580 °C, breakage of the weak bond in YQ emitted only 2.1 wt.% of the volatile matters [31], which were further identified as CO_2 and a trace amount of CH_4 by FTIR analysis in the curve (a) of Fig. 4. But at the second pyrolysis stage around 580–850 °C, cleavage of the main carbon matrix emitted 6.01 wt.% of the volatile matters [31], which was far more than that of the first pyrolysis stage, mainly due to the much higher weight content of the fixed carbon in YQ than that of the volatile matters, as shown in Table 1.

But for the reaction of YQ with reference oxides Fe_2O_3 and CuO in Fig. 3(c) and (d), respectively, two reaction stages were experienced for either the reaction of YQ with Fe_2O_3 or CuO. Two characteristic temperatures for the YQ with Fe_2O_3 at these two stages in Fig. 3(c) were resided at 523.9 and 815.1 °C with the two comparative DTG values below 0.1 wt.%/min. But the reaction of YQ with CuO changed a lot with the two characteristic temperatures shifting to the lower temperatures as 492.3 and 792.7 °C, respectively, as shown in Fig. 3(d). And the DTG value for CuO with YQ at the first stage was

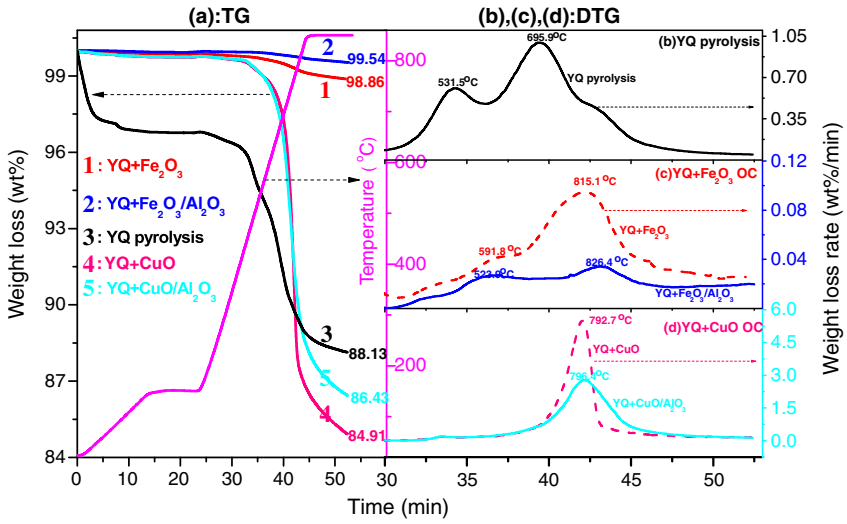

Fig. 3. Reaction of YQ with Fe_2O_3/Al_2O_3 and CuO/Al_2O_3 OCs: (a) weight loss: (b) weight loss rate of YQ pyrolysis under N_2 atmosphere; (c) weight loss rate of YQ with Fe_2O_3/Al_2O_3; and (d) weight loss rate of YQ with CuO/Al_2O_3.

nearly indiscernible and reached 0.2 wt.%/min, far less than that value at the second stage as high as 5.5 wt.%/min, indicating a higher reactivity of YQ with CuO than with Fe_2O_3. In addition, FTIR analysis of the gaseous products (mainly CO_2 and H_2O) obtained at the characteristic temperature of the first stage in Fig. 4(b) and (d) further confirmed that the reaction of YQ with Fe_2O_3 or CuO did occur at 523.9 °C and 492.3 °C, respectively. The reaction characteristic temperatures reported here were much lower than the temperatures reported by Siriwardane, et al. [21] and Cao, et al. [25], possibly due to the higher reactivity of the synthesized reference oxides in our research than those ordered from the commercial sources.

Finally, the reaction characteristics of YQ with both Fe_2O_3/Al_2O_3 and CuO/Al_2O_3 were studied. From Fig. 3(c) and (d), two reaction stages were also presented to the reaction of YQ with Fe_2O_3/Al_2O_3 or CuO/Al_2O_3 over 200 °C, similar to that YQ with those two reference oxides above. But at the first reaction stage, both the initial reaction temperatures and the characteristic temperatures for the Fe_2O_3/Al_2O_3 or CuO/Al_2O_3 with YQ were found out smaller than those corresponding reference oxides, due to the higher structural parameters (including surface area and porosity) of Fe_2O_3/Al_2O_3 or CuO/Al_2O_3 in relative to their reference oxides shown in Table 2, and thus higher reactivity obtained. At the second reaction stage, the characteristic temperature T_m of YQ with Fe_2O_3/Al_2O_3 or CuO/Al_2O_3 was delayed to 826.4 and 796.4 °C, respectively, higher than those values of YQ with reference oxide Fe_2O_3 (815.1 °C) or CuO (792.7 °C), similar to our previous experiment on the CLC of a Chinese bituminous coal with $CuFe_2O_4/Al_2O_3$ OC [32], mainly due to the hindrance of the inert Al_2O_3 to the effective contact of carbon produced from YQ with the active oxides Fe_2O_3 or CuO, in accordance with the conclusion reached by Siriwardane et al. [23].

3.2.2. Conversions of the synthesized Fe_2O_3/Al_2O_3 or CuO/Al_2O_3 with YQ

In order to reveal the interaction of YQ coal with OC, based on the TG experimental results of YQ pyrolysis and its reaction with Fe_2O_3/Al_2O_3 and CuO/Al_2O_3 OCs or their relative reference oxides in Fig. 3, two conversion indexes as the OC conversion X_{OC} for OC alone in its

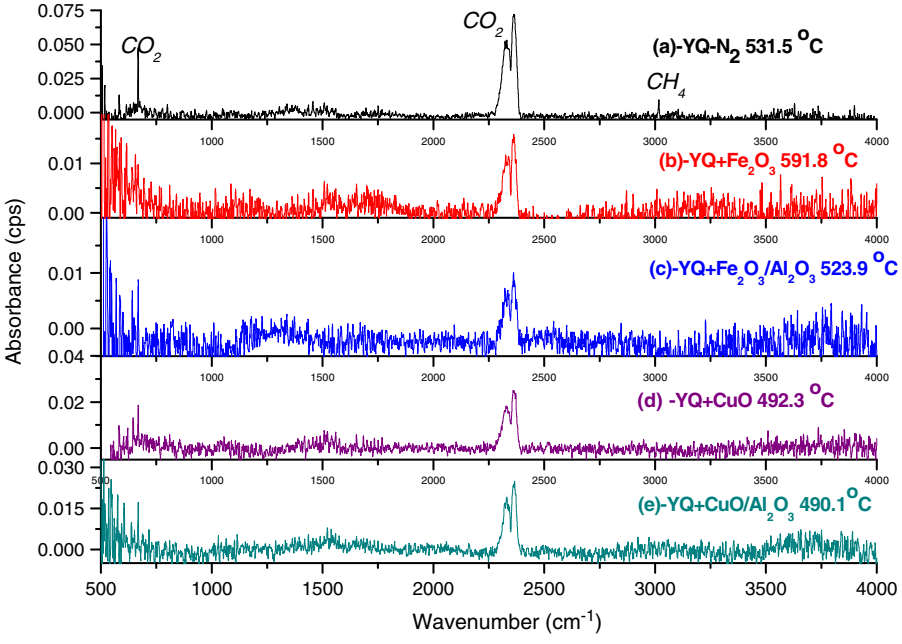

Fig. 4. FTIR spectra of gas products from the reaction of YQ with Fe_2O_3/Al_2O_3, CuO/Al_2O_3 OCs.

mixture with YQ and the mixture conversion X_{YQ+OC} for YQ with different OCs were calculated using Eqs. (4) and (7), respectively. And the calculated results are presented in Fig. 5.

From Fig. 5(a), both the mixture conversion indexes for YQ with Fe_2O_3/Al_2O_3 or its reference oxide Fe_2O_3 as $X_{Fe_2O3/Al2O3+YQ}$ or X_{Fe_2O3+YQ} were below 3%, far smaller than their corresponding indexes for CuO/Al_2O_3 or CuO with YQ over 50%, shown in Fig. 5(b) as X_{CuO/Al_2O3+YQ} or X_{CuO+YQ}, which displayed the higher reactivity of CuO based OC than that of Fe_2O_3 based OC. Therefore, with regard to its reactivity to YQ, CuO based OC was more suitable to the realistic CLC system with YQ coal as fuel, though Fe_2O_3 based OC was cheaper.

Furthermore, through the comparison of the mixture conversion indexes to their relative OC conversion indexes, the real rate-limited step for the reaction of YQ with OCs were revealed. For the reaction of YQ with Fe_2O_3 based OC, from Fig. 5(a), it would be observed that, there existed intersections between the curves for the mixture conversion index X_{Fe_2O3+YQ} and Fe_2O_3 conversion index X_{Fe_2O3} or the mixture conversion index $X_{Fe_2O3/Al2O3+YQ}$ and Fe_2O_3/Al_2O_3 conversion index $X_{Fe_2O3/Al2O3}$, respectively. Before the relative intersection points, the mixture conversion index X_{Fe_2O3+YQ} or $X_{Fe_2O3/Al2O3+YQ}$ was bigger than that of OC conversion index X_{Fe_2O3} or $X_{Fe_2O3/Al2O3}$, which implied that at these early reaction stage, the gaseous products emitted from YQ pyrolysis were sufficient and the reaction of YQ with Fe_2O_3 was determined by the slow lattice oxygen transferred from Fe_2O_3 to the gaseous products produced from YQ. After the intersection points and with the temperature increased, the opposite variation trend was presented. The mixture conversion index X_{Fe_2O3+YQ} or $X_{Fe_2O3/Al2O3+YQ}$ was smaller than that of OC conversion index X_{Fe_2O3} or $X_{Fe_2O3/Al2O3}$, which meant that the reaction of YQ with Fe_2O_3 or Fe_2O_3/Al_2O_3 was limited by the insufficient supply of gaseous products from YQ pyrolysis.

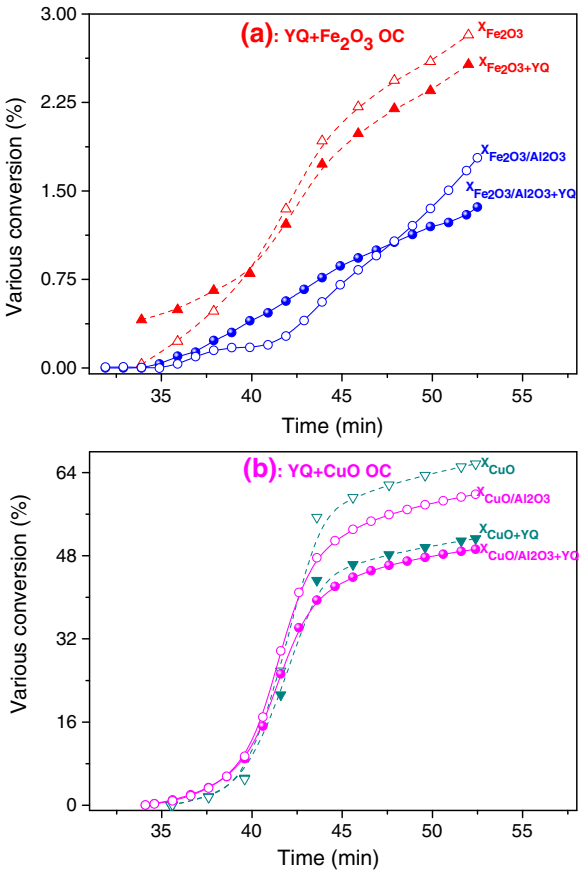

Fig. 5. Conversion indexes for the reaction of YQ with different OCs: (a)YQ + Fe_2O_3/Al_2O_3; and (b) YQ + CuO/Al_2O_3.

But for the reaction of CuO or CuO/Al_2O_3 with YQ, below 40 min in Fig. 5(b) (i.e. corresponding to 720 °C in Fig. 3(a)), the mixture conversion index of CuO with YQ as X_{CuO+YQ} or CuO/Al_2O_3 with YQ as X_{CuO/Al_2O3+YQ} was almost overlapped with the corresponding CuO conversion index X_{CuO} or CuO/Al_2O_3 conversion index X_{CuO/Al_2O3}, respectively. Therefore, at the low temperature range below 720 °C, the lattice oxygen supplied from CuO or CuO/Al_2O_3 OC nearly met the full oxidation of the gaseous products emitted from YQ pyrolysis; but later on, at the higher temperature over 720 °C, limited by YQ pyrolysis, gaseous products emitted from YQ were still not sufficient to the lattice oxygen supplied from the active CuO.

Based on the discussion above, it could be concluded that at the temperature of interest for CLC of coal over 800 °C, whether for the reaction of YQ with Fe_2O_3/Al_2O_3 or CuO/Al_2O_3 OC, the real limiting step is YQ pyrolysis and gasification instead of its reaction with the OCs used, which was in accordance with other findings [2,4,6,8,9,16,21,25,27].

3.3. Chemical and microstructure analysis

Since CuO based OC was more suitable to such a high rank coal YQ, the reaction of YQ with CuO/Al_2O_3 OC was focused in this section. To help understand the issue of ash separation from the reaction of YQ with CuO/Al_2O_3 OC and further clarify the reaction mechanisms involved, the morphology and elemental composition of the solid residues from the reaction of YQ with CuO/Al_2O_3 were characterized using FSEM-EDX, as shown in Fig. 6 and Table 4. The detailed phases for the reaction of YQ with CuO/Al_2O_3 were further identified using XRD analysis, and the results are provided in Fig. 7.

From Fig. 7(a) for the reaction of YQ with reference oxide CuO, it could be observed that in SEM pattern, the solid residues were composed of many discrete particles in different sizes from 0.1 to ~1 μm in spot 1 and the relatively gray bulk in spot 2. By the EDX analysis in Table 4, the atomic fractions of C, O, Cu and Si were not uniformly distributed. The C content in spot 2 was 21.95%, much higher than that in spot 1, possibly resulting from the main carbon matrix, which was not completely disintegrated during YQ pyrolysis. Meanwhile, the O and Si contents in spot 1 were found as 50.83% and 25.02%, respectively, greatly higher than those in spot 2, but Cu content in spot 1 was only 12.77%, nearly one quarter of that content in spot 2. According to the molar contents of these three elements Si, O and Cu in the two spots, the related species involved in spot 1 should be attributed to Cu and SiO_2, and the inherent species in spot 2 were mainly deduced as Cu and Cu_2O. These species were further verified by XRD analysis, as shown in Fig. 7(c), where the main reduced counterparts of CuO were Cu and Cu_2O and the main mineralogy compositions were identified as SiO_2, $Ca_2Al_2SiO_7$ and Al_2SiO_5 involved. In addition, from Table 4, although the residue carbon still accounted for a large fraction by EDX analysis, it could not be detected out in XRD analysis, mainly due to the amorphous characteristics of the carbon left from the reaction of YQ with CuO [33,34].

But from Fig. 7(b) for the reaction of YQ with CuO/Al_2O_3 in the SEM pattern, the sizes of the solid residues were evenly distributed with abundant pores formed, and no discernible agglomeration or sintering was observed. The bulky carbon matrix of YQ had disintegrated into smaller carbon grains. By the EDX analysis in Table 4, although the Al contents in the two optionally selected points were evenly distributed around 22–23%, but the distribution of the atomic contents for the other four elements (including C, O, Cu and Si) varied greatly, similar to the reaction of YQ with CuO. According to the molar ratios of Cu, Al and O as nearly 1:2:4 in spot 2, the species adherent to the YQ carbon grain was deduced as $CuAl_2O_4$. But in spot 1, the species were more complicated, where the active CuO was reduced into Cu and Cu_2O, whereas the actual $CuAl_2O_4$ support was not completely inert, some of $CuAl_2O_4$ involved in the CuO/Al_2O_3 OC was reduced to $CuAlO_2$ and Al_2O_3 [35–37], which were also verified by the XRD

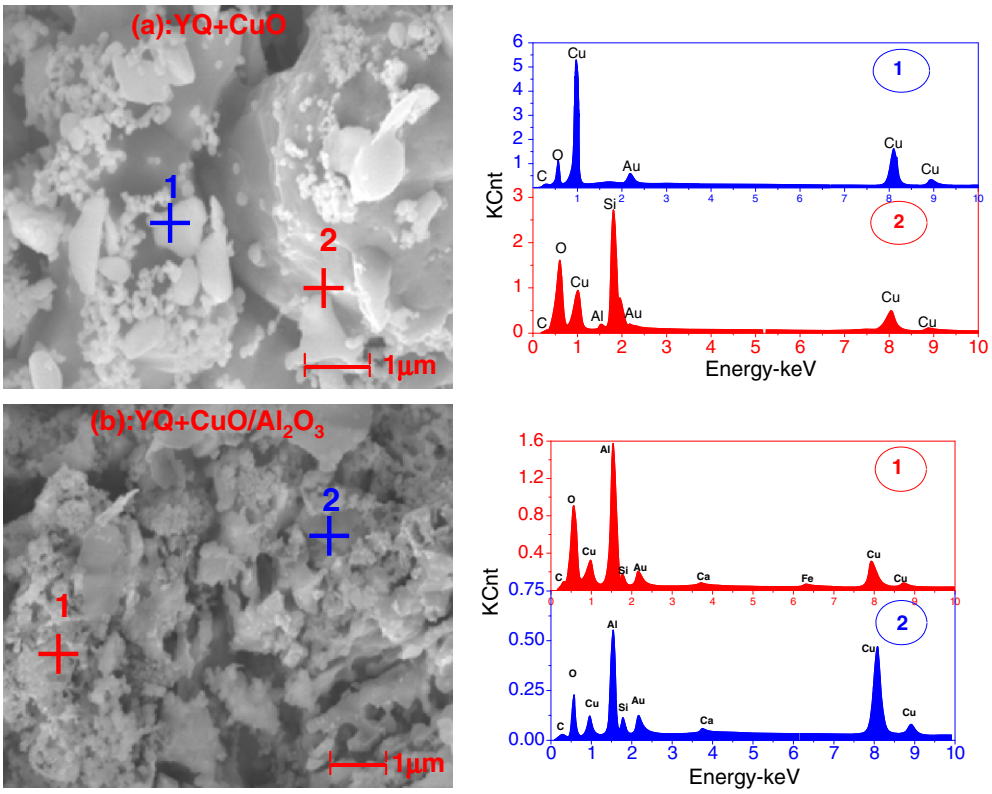

Fig. 6. FSEM-EDX analysis of YQ with CuO based OC: (a) YQ + CuO; and (b) YQ + CuO/Al_2O_3.

analysis shown in Fig. 7(d). The reason for Al_2O_3 not detected out by XRD analysis was possibly that the formed Al_2O_3 at 850 °C was in its metastable state and amorphous [38,39], as certified later.

As analyzed above, enough attention should be paid to the interaction between the reduced CuO/Al_2O_3 with the mineral in YQ, because although the active oxide CuO in the CuO/Al_2O_3 OC did not interact with the minerals in YQ, Al_2O_3 (which was obtained from the reduced $CuAl_2O_4$ support) interacted with SiO_2 in YQ and formed into inert Al_2SiO_5. As a detrimental consequence, over many cycles of the reaction of YQ with CuO/Al_2O_3 in the realistic CLC system, inert support Al_2O_3 would be gradually lost by the interaction with other minerals in coal, which brought about the lower resistance of the OC to sintering and the deteriorated reactivity of OC in CLC application.

In addition, another attention should be paid to the minerals produced from the reaction of YQ with CuO-based OC shown in Fig. 7(c) and (d), which were far different than the YQ ash from the YQ combustion in air shown in Fig. 7(b). Therefore, evolution of minerals in CLC of YQ with CuO/Al_2O_3 should be further deeply studied.

3.4. Thermodynamic investigation of the reaction of CuO/Al_2O_3 with YQ

In order to gain a comprehensive understanding of several aspects for the reduction of CuO/Al_2O_3 with YQ, including YQ conversion, oxygen transfer from the CuO/Al_2O_3 OC to YQ and the interaction between the minerals in YQ with the reduced CuO/Al_2O_3 OC, reaction of CuO/Al_2O_3 with YQ was further analyzed by the aid of thermodynamic simulation. And the simulation results are presented in Fig. 8. Meanwhile, a reference reaction of YQ with oxide CuO was also simulated in order to clarify the effect from Al_2O_3 involved in the selected OC, and the results are included in Fig. 8 for comparison as well.

3.4.1. YQ coal conversion during its reaction with CuO/Al_2O_3

Full conversion of the fuel C involved in coal to CO_2 is the primary target of CLC for easy sequestration of the CO_2 enriched in the flue gas, especially for YQ coal with the high fixed carbon content. Therefore, the conversion of C involved in YQ is the first research focus. And the equilibrium distribution of various C-containing species is provided in Fig. 8(a).

From Fig. 8(a), the solid C fraction of YQ in its reaction with CuO/Al_2O_3 or reference CuO decreased quickly with the reaction temperature increased from 400 to 1100 °C, because the enhanced temperature promoted the disintegration of the carbon matrix of YQ. And more gaseous products were emitted, among which, CO_2 was found to be dominant. But it was surprising to observe that the CO_2 fraction decreased obviously with temperature, especially for the reaction of YQ with CuO/Al_2O_3, which was not consistent

Table 4
Elemental analysis (Atomic%) of the reaction of YQ with CuO based OC by FSEM-EDX, applying ZAF correction method.

YQ +		C	O	Fe	Cu	Al	Si	S	K	Ca	Mg
CuO	Spot 1	7.89	50.83	0.18	12.77	0.82	25.02	0.2	0.08	0.2	2.02
	Spot 2	21.95	29.49	0	43.95	0.4	0.71	0.34	0.05	0	3.12
$CuO + Al_2O_3$	Spot 1	13.82	19.29	0.62	34.23	23.04	2.79	0.43	0.41	0.83	4.53
	Spot 2	21.94	40.45	0.47	10.96	22.11	1.72	0.28	0.09	0.20	1.77

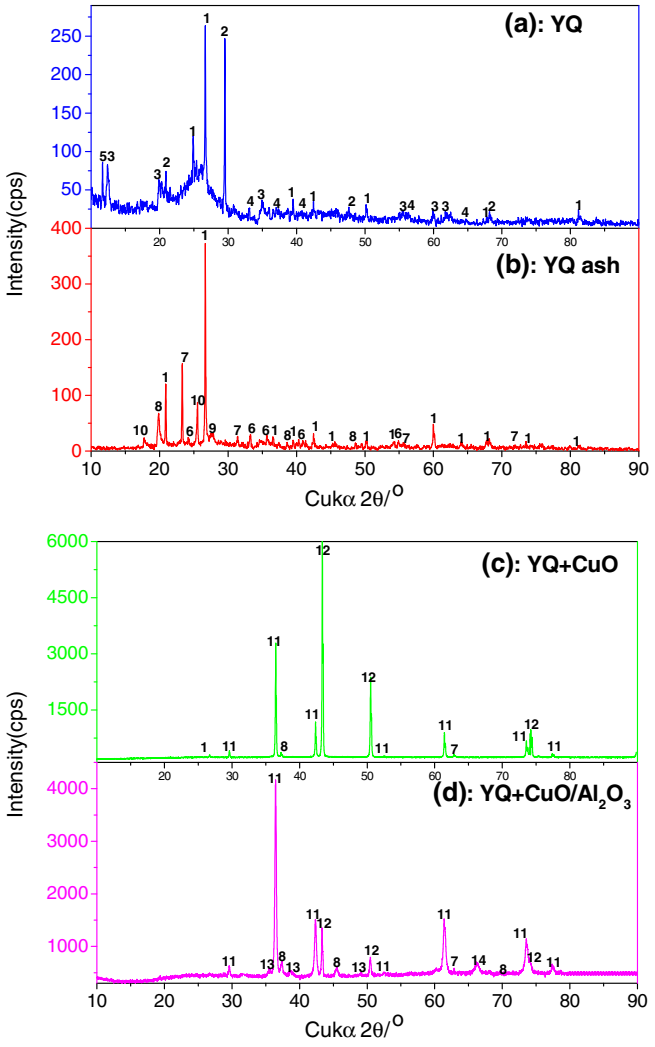

Fig. 7. XRD study of the solid products of YQ with CuO based OC.In this figure, 1: quartz [SiO_2]; 2: calcite [$CaCO_3$]; 3.kaolinite [$Al_2Si_2O_5(OH)_4$]; 4.pyrite [FeS_2]; 5.gypsum [$CaSO_4.2H_2O$]; 6.hematite [Fe_2O_3]; 7.gehlenite [$Ca_2Al_2SiO_7$] 8. Silimanite [Al_2SiO_5]; 9.albite [$NaAlSi_3O_8$]; 10.akermanite [$Ca_2MgSi_2O_7$]; 11.cuprite [Cu_2O]; 12.copper [Cu]; 13.copper aluminum oxide [$CuAl_2O_4$]; and 14. copper aluminum oxide [$CuAlO_2$].

with other experiemental results [2–4,6,7]. Three reasons should be responsible for such an observation. The first one was perhaps due to the limitation of thermodynamic analysis as pointed out above, which did not consider the kinetic constraints in the real process [30]. Another reason was that, from the thermodynamic perspective, low temperature was beneficial to the initiation of the exothermic reaction of YQ with CuO based OC [40,41]. Finally, the introduced inert Al_2O_3 should be also considered. Its interaction with CuO into less reactive $CuAl_2O_4$ would decrease the lattice oxgyen supplied to YQ, which would result in the CO fraction increased with temperature.

3.4.2. CuO/Al_2O_3 OC conversion

Oxygen supplied from OC is of great significance to the full oxidation of coal in CLC. Therefore, CuO based OC evolution and oxygen transfer were further studied. Various Cu-containing species were simulated and provided in Fig. 8(b).

From Fig. 8(b), almost all the active CuO in CuO based OC was reduced by YQ to elemental Cu with its fraction stabilized around ~99% throughout the whole temperature range in 400–1100 °C, which implied that, during the reaction of YQ with CuO or CuO/Al_2O_3, the active CuO was mainly reduced to Cu_2O and then further to Cu by transfer of the lattice oxygen [O] to YQ in a sequential pathways below [42], similar to the reduction of CuO with H_2 [43,44] or CO [42,45].

$$2CuO \rightarrow Cu_2O + [O] \quad (8)$$

$$Cu_2O \rightarrow 2Cu + [O] \quad (9)$$

Furthermore, from the enlarging insets in Fig. 8(b) for YQ with CuO or for YQ with CuO/Al_2O_3, it could be observed that either Cu_2O or $CuAlO_2$ were produced and nearly stabilized around zero below 800 °C; but over 800 °C, both of them increased rapidly. It could be inferred that below 800 °C, the sequential reduction of the spinel $CuAl_2O_4$ with YQ occurred as described in Eqs. (10) and (11), because $CuAl_2O_4$ involved in CuO/Al_2O_3 was also found to have some reduction activity, though lower than that of CuO [35,46], similar to the reduction of $CuAl_2O_4$ with H_2 [36,37] or CO [35].

$$2CuAl_2O_4 \rightarrow 2CuAlO_2 + Al_2O_3 + [O] \quad (10)$$

$$2CuAlO_2 \rightarrow 2Cu + Al_2O_3 + [O] \quad (11)$$

But over 800 °C, under the rapid increase of CO concentration shown in Fig. 8(a), O_2 partial pressure decreased quickly, which made the decomposition of CuO into Cu_2O [25,47] and $CuAl_2O_4$ into $CuAlO_2$ [48,49] initiated, and gaseous oxygen O_2 was directly emitted, which was further transferred to YQ for its direct combustion.

$$4CuO \rightarrow 2Cu_2O + O_2 \quad (12)$$

$$4CuAl_2O_4 \rightarrow 4CuAlO_2 + 2Al_2O_3 + O_2 \quad (13)$$

Finally, the main reaction pathways for YQ with CuO based OC were determined. The greater percentages of Cu as compared to those of Cu_2O and $CuAlO_2$ in Fig. 8(b) indicated that the dominant reaction pathways for the CuO with YQ should be Eq. (8) coupled with Eq. (9) other than Eq. (12). Similarly, the reduction of $CuAl_2O_4$ with YQ also inititated by the main reaction pathways of Eqs. (10) and (11) other than Eq. (13).

In addition, from Fig. 8(b) it could be found that the active CuO tended to react with various sulfur species emitted from YQ to form Cu_2S throughout the whole reaction stage, similar to the finding of others in the reaction of syngas with their sysnthesized CuO-based OC [50,51].

3.4.3. Evolution of Si and Al-containing minerals

Si and Al minerals in coal were widely distributed with larger fraction than other minerals [52]. It was the case with the ash analysis of YQ in Table 1. Therefore, the final research focus was mainly concentrated on the transformation of Si and Al minerals in YQ and their interaction with the reduced CuO/Al_2O_3. Various Si and Al species from the thermodynamic simulation for the reaction of YQ with CuO/Al_2O_3 are provided in Fig. 8(c) and (d), respectively.

As a reference, from Fig. 8(c) and (d) for the reaction of YQ with reference oxide CuO, it was observed that, for the transforamtion of various Si-containing species in Fig. 8(c), below 600 °C, the main Si-containing species were quartz (SiO_2) and prehnite ($Ca_2Al_2Si_3O_{10}(OH)_2$) with their fractions stabilized around 63.6% and 23.2%, respectively; but over 600 °C, the fraction of prehnite decreased fastly until to zero at 800 °C with the rapid increase in SiO_2 to nearly 80%. But from Fig. 8(d) for the transformation of various Al-containing species, below 600 °C, the main Al-containing species were nearly 70% of prehnite and ~26% of silimanite (Al_2SiO_5), respectively; and then over 600 °C, silimanite (Al_2SiO_5) and gehlenite ($Ca_2Al_2SiO_7$) fastly increased with their fractions stabilized around 55% and 35.2%,

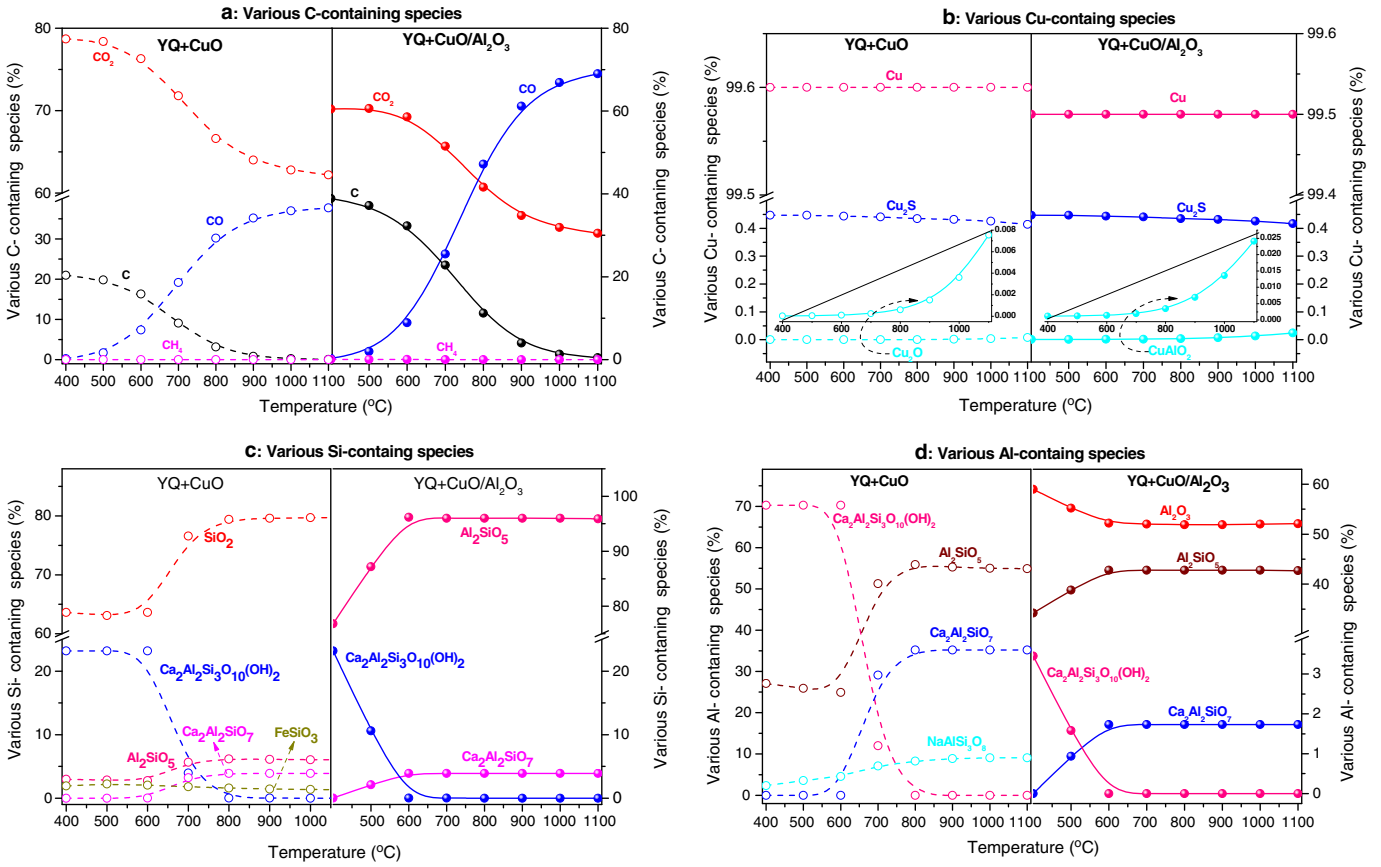

Fig. 8. Equilibrium distribution of various species for the reduction of YQ with CuO and CuO/Al_2O_3 OC, respectively:(a) Various C-containing species; (b) Cu-containing species distribution; (c) Al-containing species distribution; and (d) Si-containing species distribution.

respectively. As described above, it could be concluded that the main Si and Al species for the reaction of YQ with CuO were silimanite and prehnite below 600 °C, but over 600 °C, were quartz, silimanite and gehlenite, respectively.

Furthermore, the reaction mechanisms for the main Si and Al species formed during the reaction of YQ with CuO were explored. The observed silimanite below 600 °C could be viewed as the initial onset towards the intermediate mineral metakaolinite ($Al_2Si_2O_7$), and was most probably arising from the decomposition of kaolinite ($Al_2Si_2O_5(OH)_4$) present in the YQ coal as shown in Fig. 7(a) by XRD analysis [53–55],

$$Al_2Si_2O_5(OH)_4(\text{kaolinite}) \rightarrow Al_2SiO_5(\text{silimanite}) + SiO_2 + 2H_2O \quad (14)$$

Prehnite was found thermally stable at lower temperature below 600 °C from Fig. 8(c) and (d), which was obtained through a series of complex intermediate reactions by the gehlenite ($Ca_2Al_2SiO_7$) formation in Eq. (15) at 400–600 °C [56] or in Eq. (16) over 600 °C [57], further crystallization into anorthite ($Ca_2Al_2SiO_8$) in Eq. (17) [58], and finally interaction between the anorthite, wollastonite and excess steam (H_2O) [59,60] in Eq. (18), as described below.

$$Al_2Si_2O_5(OH)_4(\text{kaolinite}) + 2CaCO_3(\text{calcite}) \rightarrow Ca_2Al_2SiO_7(\text{gehlenite}) + SiO_2 + 2H_2O + 2CO_2 \quad (15)$$

$$Al_2Si_2O_7(\text{metakaolinite}) + (2+n)CaO \rightarrow Ca_2Al_2SiO_7(\text{gehlenite}) + nCaSiO_3(\text{wollastonite}) \quad (16)$$

$$Ca_2Al_2SiO_7(\text{gehlenite}) + 3SiO_2 + Al_2O_3 \rightarrow 2Ca_2Al_2Si_2O_8(\text{anorthite}) \quad (17)$$

$$Ca_2Al_2SiO_8(\text{anorthite}) + CaSiO_3(\text{wollastonite}) + H_2O(g) \rightarrow Ca_2Al_2Si_3O_{10}(OH)_2(\text{prehnite}) \quad (18)$$

But for the reaction YQ with CuO/Al_2O_3 in both Fig. 8(c) and (d), the transformation of the Si and Al-containing species was greatly different from the reaction of YQ with CuO discussed above. Although prehnite still existed below 600 °C and fastly decreased to zero around 800 °C, but the main Si and Al minerals for the reaction of YQ with CuO/Al_2O_3 were silimanite and free alumin oxide (Al_2O_3), respectively, which were confirmed in our previous FSEM-EDX analysis. Meanwhile, from Fig. 8(d), below 600 °C, Al_2O_3 decreased from 59% at 400 °C to 52.2% at 600 °C, acompanied by the increase of Al_2SiO_5 from 34.2% at 400 °C to 42.8% at 600 °C; but over 600 °C, both Al_2O_3 and Al_2SiO_5 were stablized ~52% and 42.8%, respectively. The observed occurrence of Al_2SiO_5 was most possibly arising from the interaction between the SiO_2 in YQ and Al_2O_3 from the reaction of YQ with CuO/Al_2O_3 in Eqs. (10) and (11) coupled with Eq. (13) [54,55].

$$Al_2O_3 + SiO_2 \rightarrow Al_2SiO_5 \quad (19)$$

4. Conclusions

Reactions of YQ anthracite with Fe_2O_3/Al_2O_3 or CuO/Al_2O_3 OC were perfomred in TGA, and then systematically investigated using different experimental means, such as FTIR, FSEM-EDX, XRD and

further analyzed by the aid of the thermodynamic simulation. Relevant conclusions were reached as followed.

(1) Both Fe_2O_3/Al_2O_3 and CuO/Al_2O_3 were synthesized using a novel SGCS method and further characterized with phase and structural analysis. The synthesized OCs were actually composed of active oxides Fe_2O_3, CuO and inert support Al_2O_3 and $CuAl_2O_4$, respectively. And for SGCS method used in this research, the introduced inert support Al_2O_3 at its mass ratio to Fe_2O_3 or CuO as 1:4 was suitable, which effectively improved the resistance of CuO or Fe_2O_3 based OC to sintering and made their reaction stability well maintained over the four redox cycles.

(2) TGA-FTIR experiments for the two reactions of YQ with Fe_2O_3/Al_2O_3 and CuO/Al_2O_3 were conducted. The results revealed that over 150 °C, two reaction stages were undergone for these two reactions at 300–600 °C and 600–850 °C, respectively. Although the two maximum weight loss rates for YQ with Fe_2O_3/Al_2O_3 were at the same magnitude and both of them below 0.035 wt.%/min, but the maximum weight loss rate for YQ with CuO/Al_2O_3 at the second stage was more pronounced and reached up to 2.8 wt.%/min.

(3) Two conversion indexes were established for the reduction of Fe_2O_3/Al_2O_3 and CuO/Al_2O_3 with YQ. The mixture conversion index of YQ with CuO/Al_2O_3 was far bigger than that of YQ with Fe_2O_3/Al_2O_3, which indicated that CuO/Al_2O_3 was more suitable to YQ in CLC. Meanwhile, both OC conversion indexes of Fe_2O_3/Al_2O_3 and CuO/Al_2O_3 were bigger than their mixture conversion indexes with YQ at the temperature of CLC interest (f.g., above 800 °C), clearly indicating that the real limiting step involved is pyrolysis and gasification of YQ itself, instead of its reaction with OCs.

(4) FSEM-EDX and XRD analysis of the solid reduced residues from YQ with CuO/Al_2O_3 indicated that the active CuO was reduced to Cu and Cu_2O, but support $CuAl_2O_4$ formed during preparation also had inferior reactivity and was reduced to $CuAlO_2$ and Al_2O_3. By combination with the thermodynamic analysis, it was found that reduction of CuO and $CuAl_2O_4$ was dominated by the transfer of lattice oxygen [O] invovled in a sequential mode by Eqs. (8) and (9) and Eqs. (10) and (11), respectively, instead of gaseous oxgyen O_2 formed in Eqs. (12) and (13) throughout the whole reaction at 400–1000 °C.

(5) The transformation of Si- and Al-containing species for the reaction of YQ with CuO/Al_2O_3 was studied. The main Si, Al minerals formed for YQ with CuO/Al_2O_3 were Al_2SiO_5 and free Al_2O_3, instead of SiO_2, Al_2SiO_5 and $Ca_2Al_2SiO_7$ over 600 °C for YQ with the reference oxide CuO.

Acknowledgments

This work is supported by the A*Star SERC Grant of Singapore (SERC 0921380025-M47070019), National Natural Science Foundation of China (Nos. 50906030 and 50936001), Chinese Postdoctoral Science Foundation (20110491135) and partial funding from National Basic Research Program (2010CB227003, 2011CB707301). Meanwhile, the staffs from the Analytical and Testing Center, Huazhong University of Science and Technology, were appreciated for the related experimental analysis.

References

[1] H. Jin, T. Okamoto, M. Ishida, Development of a novel chemcial-looping combustion: synthesis of a solid material $NiO/NiAl_2O_4$, Industrial & Engeering Chemistry Research 38 (1) (1999) 126–132.
[2] N. Berguerand, A. Lyngfelt, Design and operation of a 10 kWth chemical-looping combustor for solid fuels — testing with South African coal, Fuel 87 (12) (2008) 2713–2726.
[3] H. Leion, T. Mattisson, A. Lyngfelt, Solid fuels in chemical-looping combustion, International Journal of Greenhouse Gas Control 2 (2) (2008) 180–193.
[4] L.H. Shen, J.H. Wu, Z.P. Gao, J. Xiao, Experiments on chemical looping combustion of coal with a NiO based oxygen carrier, Combustion and Flame 156 (3) (2009) 721–728.
[5] K. Mahalatkar, J. Kuhlman, E.D. Huckaby, T. O'Brien, CFD simulation of a chemical-looping fuel reactor utilizing solid fuel, Chemical Engineering Science 66 (16) (2011) 3617–3627.
[6] L.H. Shen, J.H. Wu, Z.P. Gao, J. Xiao, Reactivity deterioration of NiO/Al_2O_3 oxygen carrier for chemical looping cmbustion of coal in 10 kW_{th} reactor, Combustion and Flame 156 (7) (2009) 1377–1385.
[7] H. Leion, E. Jerndal, B.M. Steenari, S. Hermansson, T. Mattisson, A. Lyngfelt, Solid fuels in chemical looping combustion using oxide scale and unprocessed iron ore oxygen carriers, Fuel 88 (10) (2009) 1945–1954.
[8] J.S. Dennis, S.A. Scott, In situ gasification of a lignite coal and CO_2 separation using chemical looping with a Cu-based oxygen carrier, Fuel 89 (7) (2010) 1623–1640.
[9] J.S. Dennis, C.R. Müller, S.A. Scott, In situ gasification and CO_2 separation using chemical looping with a Cu-based oxygen carrier: performance with bituminous coals, Fuel 89 (9) (2010) 2353–2364.
[10] H.W. Dai, Y.Y. Zhang, K.Y. Xie, W.L. Wang, Anthracite coal: resources and market outlook, China Coal 25 (1–2) (1999) 17–21 (in Chinese).
[11] Y.-M. Ren, Anthracite resources and properties of China, Clean Coal Technology 10 (3) (2004) 8–10 (in Chinese).
[12] J.M. Andresen, C.E. Burgess, P.J. Pappano, H.H. Schobert, New directions for non-fuel uses of anthracites, Fuel Processing Technology 85 (12) (2004) 1373–1392.
[13] M. Johansson, T. Mattisson, A. Lyngfelt, Comparison of oxygen carriers for chemical-looping combustion, Journal of Thermal Science 10 (3) (2006) 93–107.
[14] B.W. Wang, R. Yan, D.H. Lee, Y. Zheng, H.B. Zhao, C.G. Zheng, Characterization and evaluation of Fe_2O_3/Al_2O_3 oxygen carrier prepared by sol–gel combustion synthesis, Journal of Analytical and Applied Pyrolysis 91 (1) (2011) 105–113.
[15] C. Saha, B. Roy, S. Bhattacharya, Chemical looping combustion of Victorian brown coal using NiO oxygen carrier, International Journal of Hydrogen Energy 36 (4) (2011) 3253–3259.
[16] H.B. Zhao, L.M. Liu, B.W. Wang, D. Xu, L.L. Jiang, C.G. Zheng, Sol–gel-derived $NiO/NiAl_2O_4$ oxygen carriers for chemical-looping combustion by coal char, Energy & Fuels 22 (2) (2008) 898–905.
[17] J.B. Yang, N.S. Cai, Z.S. Li, Reduction of iron oxide as an oxygen carrier by coal pyrolysis and steam char gasificaiton intermediate products, Energy & Fuels 21 (6) (2007) 3360–3368.
[18] Y. Cao, W.-P. Pan, Investigation of chemical looping combustion by solid fuels. 1. Proces analysis, Energy & Fuels 20 (5) (2006) 1836–1844.
[19] M.K. Chandel, A. Hoteit, A. Delebarre, Experimental investigation of some metal oxides for chemical looping combustion in a fluidized bed reactor, Fuel 88 (5) (2009) 898–908.
[20] S.Y. Chuang, J.S. Dennis, A.N. Hayhurst, S.A. Scott, Development and performance of Cu-based oxygen carriers for chemical-looping combustion, Combustion and Flame 154 (1–2) (2008) 109–121.
[21] R. Siriwardane, H.J. Tian, G. Richards, T. Simonyi, J. Poston, Chemical-looping combustion of coal with metal oxide oxygen carriers, Energy & Fuels 23 (8) (2009) 3885–3892.
[22] E.M. Eyring, G. Konya, J.S. Lighty, A.H. Sahir, A.F. Sarofim, K. Whitty, Chemical looping combustion with copper oxide as carrier and coal as fuel, Oil&Gas Science and Technology 66 (2) (2011) 1–13.
[23] R. Siriwardane, H.J. Tian, D. Miller, G. Richards, T. Simonyi, J. Poston, Evaluation of reaction mechanism of coal-metal oxide interactions in chemcial-looping combustion, Combustion and Flame 157 (11) (2010) 2198–2208.
[24] H.M. Gu, L.H. Shen, J. Xiao, S.W. Zhang, T. Song, Chemical looping combustion of biomass/coal with natural iron ore as oxygen carrier in a continuous reactor, Energy & Fuels 25 (1) (2011) 446–455.
[25] Y. Cao, B. Casenas, W.-P. Pan, Investigation of chemical looping combustion by solid fuels. 2. Redox reaction kinetics and product characterization with coal, biomass, and solid waste as solid fuels and CuO as an oxygen carrier, Energy & Fuels 20 (5) (2006) 1845–1854.
[26] S. Mookherjee, H.S. Ray, A. Mukherjee, Thermogravimetric studies on the reduction of hematite ore fines by a surrounding layer of coal or char fines. Part 2. Non-isothermal kinetic studies, Thermochimica Acta 95 (1) (1985) 247–256.
[27] X.Y. Sun, W.G. Xiang, S. Wang, W.D. Tian, X. Xu, Y.J. Xu, Y.H. Xiao, Investigation of coal fueled chemical looping combustion using Fe_3O_4 as oxygen carrier: influence of variables, Journal of Thermal Science 19 (3) (2010) 266–275.
[28] B.W. Wang, R. Yan, H.B. Zhao, Y. Zheng, Z.H. Liu, C.G. Zheng, Investigation of chemical looping combustion of coal with $CuFe_2O_4$ oxygen carrier, Energy & Fuels 25 (17) (2011) 3344–3354.
[29] C. Saha, S. Bhattacharya, Comparison of CuO and NiO as oxygen carrier in chemical looping combustion of a Victorian brown coal, International Journal of Hydrogen Energy 36 (18) (2011) 12048–12057.
[30] B.W. Wang, R. Yan, D.H. Lee, D.T. Liang, Y. Zheng, H.B. Zhao, C.G. Zheng, Thermodynamic investigation of carbon deposition and sulfur evolution in chemical looping combustion with syngas, Energy & Fuels 22 (2) (2008) 1012–1020.
[31] H.P. Yang, H.P. Chen, F.D. Ju, R. Yan, S.H. Zhang, Influence of pressure on coal pyrolysis and char gasification, Energy & Fuels 21 (6) (2007) 3165–3170.
[32] B.W. Wang, Y. Zheng, Z.H. Liu, H.B. Zhao, C.G. Zheng, R. Yan, Investigation of chemical looping combustion of coal with Fe_2O_3-based combined oxygen carrier, Journal of Engineering Thermophysics 31 (8) (2010) 1427–1430.
[33] K.-S. Kang, C.-H. Kim, W.-C. Cho, K.-K. Bae, S.-W. Woo, C.-S. Park, Reduction characteristics of $CuFe_2O_4$ and Fe_3O_4 by methane; $CuFe_2O_4$ as an oxidant, International Journal of Hydrogen Energy 33 (17) (2008) 4560–4568.

[34] K.-S. Kang, C.-H. Kim, K.-K. Bae, W.-C. Cho, W.-J. Kim, Y.-H. Kim, S.-H. Kim, C.-S. Park, Redox cycling of CuFe2O4 supported on ZrO2 and CeO2 for two-step methane reforming/water splitting, International Journal of Hydrogen Energy 35 (2) (2010) 568–576.
[35] M.-F. Luo, P. Fang, M. He, Y.-L. Xie, In situ XRD, Raman, and TPR studies of CuO/Al_2O_3 catalysts for CO oxidation, Journal of Molecular Catalysis A: Chemical 239 (1–2) (2005) 243–248.
[36] V. Patrick, G. Gavalas, Structure and reduction of mixed copper-aluminate oxide, Journal of American Ceramic Society 73 (2) (1990) 358–369.
[37] I.M. Plyasova, T.M. Yur'eva, I.Y. Molina, T.A. Kriger, Dynamics of structural transformations in the reduction of copper aluminate, Kinetics and Catalysis 41 (3) (2000) 429–436.
[38] I. Levin, D. Brandon, Metastable alumina polymorphs: crystal structures and transition sequences, Journal of American Ceramic Society 81 (8) (1998) 1995–2012.
[39] M.I.F. Macedo, C.A. Bertran, C.C. Osawa, Kinetics of the γ→α-alumina phase transformation by quantitative X-ray diffraction, Journal of Materials Science 42 (8) (2007) 2830–2836.
[40] K. Svoboda, G. Slowinski, J. Rogut, D. Baxter, Thermodynamic possibilities and constraints for pure hydrogen production by iron based chemical looping process at low temperature, Energy Conversion and Management 48 (12) (2007) 3063–3073.
[41] K. Svoboda, A. Siewioreka, D. Baxter, J. Rogut, M. Pohořel, Thermodynamic possibilities and constraints for pure hydrogen production by a nickel and cobalt-based chemical looping process at lower temperatures, Energy Conversion and Management 49 (2) (2008) 221–231.
[42] S.Y. Chuang, J.S. Dennis, A.N. Hayhurst, S.A. Scott, Kinetics of the chemical looping oxidation of CO by a co-precipitated mixture of CuO and Al_2O_3, Proceedings of the Combustion Institute 32 (2) (2009) 2633–2640.
[43] J.A. Rodrigueze, J.Y. Kim, J.C. Hanson, M. Perez, A.I. Frenkel, Reduction of CuO in H2: in situ time-resolved XRD studies, Catalysis Letters 85 (3–4) (2003) 247–254.
[44] J.Y. Kim, J.A. Fodriguez, J.C. Hanson, A.I. Frenkel, P.L. Lee, Reduction of CuO and Cu_2O with H_2: H embedding and kinetics effects in the formation of suboxides, Journal of American Chemistry Society 125 (35) (2003) 10684–10692.
[45] X.Q. Wang, J.C. Hanson, A.I. Frenkel, J.-Y. Kim, J.A. Rodriguez, Time-resolved studies for the mechanism of reduction of copper oxides with carbon monoxide: complex behavior of lattice oxygen and the formation of suboxides, Journal of Physical Chemistry B 108 (36) (2004) 13667–13673.
[46] S.N. Fang, P.Y. Lin, Y.L. Fu, A study of the dispersed states of copper species on $CuO/\gamma\text{-}Al_2O_3$ catalysts, Journal of Molecular Catalysis (China) 8 (2) (1994) 86–90.
[47] T. Mattisson, A. Lyngfelt, H. Leion, Chemical-looping with oxygen uncoupling for combustion of solid fuels, International Journal of Greenhouse Gas Control 3 (1) (2009) 11–19.
[48] K.T. Jacob, C.B. Alcock, Thermodynamic of $CuAlO_2$ and $CuAl_2O_4$ and phase equlibria in the system Cu_2O–CuO–Al_2O_3, Journal of American Ceramic Society 58 (5–6) (1975) 192–195.
[49] T. Tsuchida, R. Furuichi, T. Sukegawa, M. Furudate, T. Ishii, Thermoanalytical study on the reaction of the CuO–Al2O3 (η, γ and α) systems, Thermochimica Acta 78 (1–3) (1984) 71–80.
[50] R.D. Solunke, G. Veser, Integrating desulfurization with CO_2-capture in chemical-looping combusiton, Fuel 90 (2) (2011) 608–617.
[51] H.J. Tian, T. Simonyi, J. Poston, R. Siriwardane, Effect of hydrogen sulfide on chemical looping combustion of coal-derived synthesis gas over bentonite-supported metal-oxide oxygen carriers, Industrial & Engeering Chemistry Research 48 (18) (2009) 8418–8430.
[52] S.V. Vassilev, C.G. Vassileva, Occurrence, abundance, and origin of minerals in coals and coal ashes, Fuel Processing Technology 48 (2) (1996) 85–106.
[53] B. Alpern, J. Nahuys, L. Martinez, Mineral matter in ashy and non-washable coals — its influence on chemical properties, Symposium on Gondwana Coals—Proceedings and Papers. Lispon, Portugal, 1984.
[54] J.C. van Dyk, S. Melzer, A. Sobiecki, Mineral matter transformation during Sasol-Lurgi fixed bed dry bottom gasification — utilization of HT-XRD and FactSage modelling, Minerals Engineering 19 (10) (2006) 1126–1135.
[55] J.C. van Dyk, F.B. Waanders, J.H.P. van Heerden, Quantification of oxygen capture in mineral matter during gasification, Fuel 87 (12) (2008) 2735–2744.
[56] R.C. Mackenzie, A.A. Rahman, Interaction of kaolinite with calcite on heating. 1. Instrumental and procedural factors for one kaolinite in air and nitrogen, Thermochimica Acta 121 (1987) 51–69.
[57] K. Traoré, T.S. Kabré, P. Blanchart, Low temperature sintering of a pottery clay from Burkina Faso, Applied Clay Sciences 17 (5–6) (2000) 279–292.
[58] K. Traoré, P. Blanchart, Structural transformation of a kaolinite and calcite mixture to gehlenite and anorthite, Journal of Materials Chemistry 18 (2) (2003) 475–481.
[59] J.L. Haas Jr., G.R. Robinson Jr., B.S. Hemingway, Thermodynamic tabulations for selected phases in the system CaO–Al_2O_3–SiO_2–H_2O at 101.325 kPa (1atm) between 273.15 and 1800 K, Journal of Physical Chemistry Reference Data 10 (3) (1981) 575–669.
[60] J.G. Liou, Synthesis and stability relations of prehnite, $Ca_2Al_2Si_3O_{10}(OH)_2$, The American Mineralogist 56 (5–6) (1971) 507–531.